Nonrobustness of the two-dimensional turbulent inverse cascade

R. K. Scott

Northwest Research Associates, Bellevue, Washington 98007, USA

The inverse energy cascade in two-dimensional Navier-Stokes turbulence is examined in the quasisteady regime, with small-scale, band-limited forcing at scale k_f^{-1}, with particular attention to the influence of forcing Reynolds number Re on the energy distribution at large scales. The strength of the inverse energy cascade, or fraction of energy input that is transferred to larger scales, increases monotonically toward unity with increasing $\mathrm{Re} \propto k_{\max}^2/k_f^2$, where $k_{\max}$ is the maximum resolved wave number. Moreover, as Re increases beyond a critical value, for which a direct enstrophy cascade to small scales is first realized, the energy spectrum in the energy-cascading range steepens from a $k^{-5/3}$ to k^{-2} dependence. The steepening is interpreted as the result of a greater tendency for coherent vortex formation in cases when forcing scales are adequately resolved. In spectral space, it is associated with nonlocality of the inverse energy transfer.

The dual cascade of energy and enstrophy in two-dimensional turbulence is one of the most remarkable features of fluid dynamics and has been studied intensively since the pioneering work of Kraichnan and Batchelor [1,2]. Through advective nonlinearity, energy input at a given scale is transferred to ever larger scales (the inverse energy cascade) while enstrophy, or mean squared vorticity, is transferred to ever smaller scales (the direct enstrophy cascade) where it is eventually dissipated. Assuming constant energy and enstrophy fluxes ε and η, respectively, in the two inertial ranges, dimensional analysis predicts that the energy spectrum takes the form $E(k) = C\varepsilon^{2/3}k^{-5/3}$ for $k < k_f$ and $E(k) = C\eta^{2/3}k^{-3}$ for $k > k_f$, where k_f is the wave number of the forcing. Many numerical and experimental studies have provided support for these scalings in both the inverse [3–9] and direct [10–13] cascades. For reasons of computational efficiency or experimental limitations, however, most of these studies have considered the case when only one or other cascade is present. In this paper, we consider the case when both inertial ranges are present simultaneously, and examine more carefully how the energy distribution in the inverse cascade depends on the presence of the enstrophy cascade.

To produce as wide an inertial range as possible, numerical simulations of the continuously forced inverse cascade typically input energy at scales close to the smallest resolved scale in the model. The ratio $k_{\max}/k_f$ is typically in the range 1–4, where $k_{\max}$ is the maximum resolved wave number and k_f is the wave number of the forcing. As a consequence the scales at which vorticity is created are inherently underresolved by the numerical scheme: in the case of the Navier-Stokes equations the direct enstrophy cascade is eliminated and forcing is effectively within the dissipation range [14,15]. When ordinary viscosity is replaced by hyperviscosity, a short direct enstrophy cascade can appear but the flow at scales k_f^{-1} remains poorly resolved [5,16,17].

Figure 1 compares the vorticity field between cases with $k_{\max}/k_f = 8$ and $k_{\max}/k_f = 64$, with axes scaled so that k_f^{-1} is the same in each picture. The case $k_{\max}/k_f = 64$, in which the forcing is well resolved, shows a rich vorticity structure at scales well below k_f^{-1}, with filamentation and the formation of smaller coherent vortices, in contrast to the viscous ap-

pearance of the case $k_{\max}/k_f = 8$. At large scales, there is a noticeable difference in the character of the vortex population, with more intense vortices for $k_{\max}/k_f = 64$. Statistical theories of the direct enstrophy cascade have been proposed that take into account the presence of coherent vorticies [18–20]. The presence of coherent vorticies at large scales suggests that similar considerations may apply to the inverse cascade.

Most studies of the inverse cascade have focused on the steady state regime where a dissipation mechanism such as linear friction or scale-selective hypodiffusion removes energy at large scales. However, large-scale dissipation typically alters the characteristics of the inverse cascade. By removing energy at all scales, linear friction prevents a constant energy flux through the inertial range, while hypodiffusion is known to lead to a bottleneck effect and the steepening of the energy spectrum at large scales [6,16,21]. To avoid these complications, we consider here the quasisteady regime as an approximation of the infinite domain, and consider only times before significant energy has reached the domain scale.

The quasisteady regime was considered recently by Tran and Bowman [14], who considered the effect of Reynolds number Re on the strength r of the inverse cascade, defined as the fraction of energy input that cascades to larger scales. Their numerical simulations covered over a decade range of Re, all for the case $k_{\max}/k_f = 8$, for which r reached a maximum value of 0.4. Within this range r was found to vary with log Re, and a robust $k^{-5/3}$ energy spectrum was found, even at very small r, providing an explaination for the robustness of previous simulations of the inverse cascade (above references). They also constructed rigorous bounds on the enstrophy flux to small scales and showed that no direct cascade is possible unless $r \sim 1$. As they concluded, open questions remain as to the dependence of r at larger Re, and at what Re a direct cascade is realized. Here, we present a series of numerical simulations to address these questions.

We consider the two-dimensional incompressible Navier-Stokes equations in a periodic domain with a small-scale stochastic forcing f:
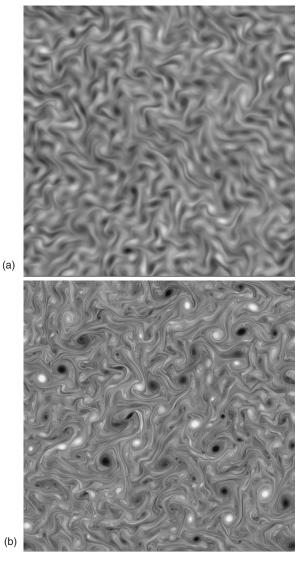
(a)

(b)

FIG. 1. Snapshot of the vorticity field $\zeta(x,y)$ at quasiequilibrium for $k_{max}/k_f=$ (a) 8 and (b) 64 (where $k_{max}=N/3$). The spatial domain shown is $|x,y| \leq 21\pi/k_f$, so the forcing scale appears the same in each panel.

$$\partial_t \omega + J(\psi, \omega) = \nu\Delta\omega + f \qquad (1)$$

where $\omega=\Delta\psi$ is the vorticity, ψ is the stream function, $J(\psi,\omega)=\psi_x\omega_y - \omega_x\psi_y$, and ν is the kinematic viscosity. The forcing f is δ correlated in time and satisfies $\langle \hat{f}(\mathbf{k})\hat{f}(\mathbf{k})^* \rangle = F(k)/\pi k$, where $\hat{f}$ is the Fourier transform of f and where the forcing spectrum $F(k)=\varepsilon$ for $|k-k_f| \leq \Delta k=2$ and $F=0$ otherwise. We solve (1) using a standard pseudospectral model with full two-thirds spectral dealiasing, so $k_{max}=N/3$ where N is the grid resolution in x and y. A fourth-order Runga-Kutta scheme is used for the time stepping, with forcing and dissipation terms treated implicitly. Multiplying (1) by ψ and integrating yields the energy equation

$$\dot{\mathcal{E}} = \varepsilon - 2\nu\mathcal{Z} \qquad (2)$$

where $\mathcal{E}=\frac{1}{2}\int d\mathbf{x}|\nabla\psi|^2 = \int_0^\infty dk\, E(k)$ is the total energy, with spectrum $E(k)$, and $\mathcal{Z}=\frac{1}{2}\int d\mathbf{x}\,\omega^2 = \int_0^\infty dk\, Z(k)$ is the enstrophy.
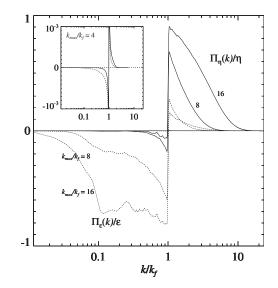

FIG. 2. Energy and enstrophy flux for $k_{max}/k_f=4,8,16$ ($k_f=85$, $N=3k_{max}=1024,2048,4096$). Inset: $k_{max}/k_f=4$ on rescaled axes.

We consider the quasistationary case where $\partial E/\partial t=0$ in the inertial range $k_p < k < k_f$, where k_p is the wave number of the energy peak. Following [14], we define the strength of the inverse cascade as $r=(\varepsilon-2\nu\mathcal{Z})/\varepsilon$ and consider the dependence of r on $\mathrm{Re}=(2\pi)^2(k_{max}/k_f)^2\mathcal{Z}^{1/2}/\nu_0$, where $\nu_0=k_{max}^2\nu$ is the diffusion rate at the smallest resolved wave number k_{max}. Here, we extend the range of Re by allowing the ratio k_{max}/k_f to increase. Because we consider simulations with different k_f, we consider forcing with a constant rate of enstrophy input, $\eta=k_f^2\varepsilon$, which allows a constant value of ν_0 to be used at different k_f and k_{max}; thus in the simulations described next, $\mathrm{Re}\propto(k_{max}/k_f)^2$.

Figure 2 shows the energy and enstrophy fluxes for three simulations with $k_{max}/k_f=4,8,16$. The strength of the inverse cascade can be estimated from the graph as minus the level of the plateau of Π_ε at $k < k_f$; the energy dissipation $\varepsilon_D=2\nu\mathcal{Z}$ is the difference between this level and the jump in Π_ε at k_f. For $k_{max}/k_f=4$, the inverse cascade is exceedingly weak, with $r \sim 10^{-4}$. The vorticity field in physical space (not shown) is dominated by diffuse vortices at the scale k_f^{-1}; there is no enstrophy cascade through filamentation, nor accumulation of energy at large scales visible in the physical fields. Despite the weakness of the inverse cascade, the energy spectrum nevertheless exhibits a clear $k^{-5/3}$ shape (Fig. 3, dashed line) consistent with the analysis of [14]. As k_{max}/k_f increases, so too does r. At $k_{max}/k_f=8$, corresponding to the upper panel in Fig. 1, $r \approx 0.3$, the inverse cascade is still weak and there is no direct cascade: the shape of the energy spectrum at $k > k_f$ remains steeper than k^{-5} [15]. Again $E \sim k^{-5/3}$ at $k < k_f$. Note from Figs. 2 and 3 that the energy has not yet reached the largest (domain) scales. Spectra plotted at different times indicate similar levels of $E(k)$ in the range $k_p < k < k_f$.

A strong inverse cascade emerges for $k_{max}/k_f=16$, for which $r \approx 0.7$. At this point the spectral shape for $k > k_f$ is shallower than k^{-5} (Fig. 3) indicating the onset of a direct cascade, although it can be seen in Fig. 2 that an inertial range with constant enstrophy flux is not fully developed.
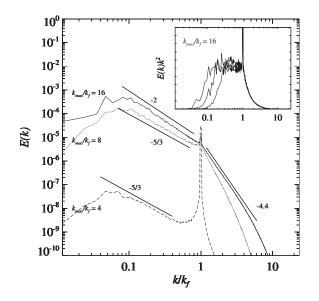
FIG. 3. Energy spectrum for the cases shown in Fig. 2. Inset: $k^2 E(k)$ for the case $k_{\max}/k_f = 16$ at three separate times.

FIG. 4. Energy spectrum for $k_{\max}/k_f = 16$ but with $k_f = 170$ and $N = 8192$. Inset: $k^2 E(k)$ (solid) and $k^{5/3} E(k)$ (dashed).

What is more interesting, however, is the change in the behavior of the inverse cascade at $k < k_f$, where it is seen that the energy spectrum has steepened to a k^{-2} dependence. Note that the k^{-2} dependence is not a transient feature, but persists as the energy front approaches the domain scale (see the compensated spectra in the inset to Fig. 3).

For $k_{\max}/k_f > 16$ the energy spectrum in the enstrophy cascading range shallows further, while the spectrum in the energy cascading range remains near k^{-2}. The case $k_{\max}/k_f = 64$ shown in Fig. 1 has $E(k) \sim k^{-3.6}$ at $k > k_f$ and $E(k) \sim k^{-2}$ at $k < k_f$ (not shown), although here $k_f = 21$ means the inverse cascade is less than a decade long and close to the domain scale. Nevertheless, the energy and enstrophy fluxes are reasonably constant over these ranges, and close to unity.

To verify that the steeper slope is not a finite size effect, Fig. 4 shows a higher-resolution case with $N = 8192$ and $k_f = 170$ ($k_{\max}/k_f = 16$). Again the k^{-2} slope is present. There is a decade between k_p and the domain scale and the energy at the domain scale is three orders of magnitude lower than the peak. As before, $E(k) \sim k^{-4.5}$ in the direct cascade. The energy spectra compensated by $k^{5/3}$ and k^2 shown in the inset on a log-linear scale highlight the k^{-2} dependence.

Using hyperviscosity of the form $\nu \Delta^\gamma$ in place of $\nu \Delta$ in (1), where $\gamma > 1$ allows higher Re to be reached. Repeating the case $k_{\max}/k_f = 64$ with $\gamma = 4$ results in $r \approx 1$ with $E \sim k^{-3.2}$ at $k > k_f$, while $E \sim k^{-2}$ persists at $k < k_f$ (not shown). There is no indication that the direct cascade has converged and previous studies indicate a k^{-3} dependence (with possible logarithmic correction) is attained at higher $k_{\max}/k_f$ [10–12]; Lindborg and Alvelius obtained a clean k^{-3} dependence using $\gamma = 2$ and forcing at $k_f = 7$, giving $k_{\max}/k_f = 1365/7 = 195$ [10].

Results from a number of different cases are summarized in Fig. 5. The filled circles correspond to the cases shown in Figs. 2 and 3, and the open circles correspond to a similar series but with forcing at $k_f = 21$. There is good agreement between the two series at a given Re (cases with $k_{\max}/k_f = 8, 16$) in terms of both r and the slopes of the inertial
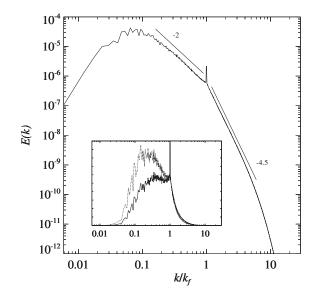
ranges. The hyperdiffusion case with $k_{\max}/k_f = 64$ and $\gamma = 4$ shows a perfect ($r = 1$) inverse cascade. For that case Re has been estimated as $\mathrm{Re} = (2\pi)^2 (k_{\max}/k_f)^2 (\mathcal{Z}^{1/2}/\nu_0)^{1/\gamma}$, which appears reasonable based on extrapolation of the Navier-Stokes cases and suggests that the use of hyperdiffusion here is roughly equivalent to a doubling of the effective resolution. Most previous studies of the inverse cascade have used $\gamma > 1$ but with $k_{\max}/k_f$ in the range 1–4 [5,6,16,17]. These studies obtained a $k^{-5/3}$ dependence in the inverse cascade as well as a direct cascade, in apparent contradiction to the present results. The direct cascade in those cases, however, is not physically realized due to numerical truncation, since at low $k_{\max}/k_f$, filamentation and the development of coherent structures are unresolved, regardless of the order of diffusion. Previous studies with larger $k_{\max}/k_f$ show steeper spectra: Fig. 2(a) of [9] is almost exactly k^{-2}, while Fig. 4 of [22] is near $k^{-2.2}$. Note that a dual cascade may be possible when frictional effects allow a steady state [23].

On dimensional grounds, a k^{-2} energy spectrum should scale as $E(k) \sim \varepsilon^{1/2} \eta^{1/6} k^{-2}$, where the constant of proportionality has here been estimated to be order unity. Here, a small
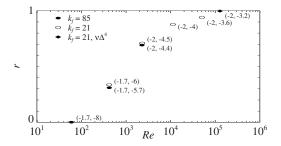

FIG. 5. Inverse cascade strength, $r = (\varepsilon - 2\nu \mathcal{Z})/\varepsilon$ against Re for $4 \leqslant k_{\max}/k_f \leqslant 64$ ($512 \leqslant N \leqslant 4096$). Numbers indicate the slopes of inverse and direct cascades. Open circles, $k_f = 21$; filled circles, $k_f = 85$; diamond represents a hyperdiffusion case with $k_f = 21$ and $N = 4096$, for which r is defined as the average Π_ε in the inverse cascading regime normalized by ε.

enstrophy flux η to large scales is necessary since the enstrophy spectrum $Z(k) \sim k^0$ extends to smaller k with increasing time (k_p decreases). This is observed in our large k_{max}/k_f simulations. Physically, a negative enstrophy flux at $k < k_f$ is consistent with an inverse cascade mediated by vortex merger in which peak vorticity is quasiconserved. In spectral space, this is related to the nonlocality of the inverse cascade, which was shown by [24] to involve energy transfer from wave numbers $k > k_f$. As argued by Borue [16], resolution of forcing scales is important in determining the vorticity distribution at larger scales. In the simulations presented here, $k_{max}/k_f \gtrsim 16$ results in a more intermittent vorticity field, and strong departures from a Gaussian distribution, as shown in Fig. 6. The broad tails are the result of coherent vortex structures, which dominate the energy and enstrophy at large k_{max}/k_f. Decomposing the vorticity field into background and coherent components following [16], reveals that the background vorticity retains a $k^{-5/3}$ energy spectrum.

In conclusion, in considering the resolution of forcing scales in two-dimensional Navier-Stoles turbulence, we have shown the existence of a transition around $k_{max}/k_f = 16$, where (i) the direct cascade first emerges [i.e., $E(k) > k^{-5}$] and (ii) the energy spectrum in the inverse energy cascade steepens to a k^{-2} dependence. At larger k_{max}/k_f, the strength of the inverse cascade approaches $r = 1$, the energy spectrum in the direct cascade shallows toward k^{-3}, while the spectrum in the indirect cascade remains near k^{-2}. The steepening in the inverse cascade is associated with the dominance of coherent vortices, which are able to form more readily when forcing scales are correctly resolved. Thus, the form of the
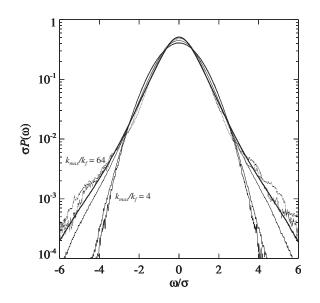

FIG. 6. Vorticity probability distribution function, normalized by standard deviation, for cases $k_{max}/k_f = 4, 8, 16, 32, 64$: $k_f = 85$ (solid), 21, (dotted), and 170 (bold).

inverse energy cascade depends on whether it appears in isolation or concurrent with a direct enstrophy cascade.

[1] R. H. Kraichnan, Phys. Fluids **10**, 1417 (1967).
[2] G. K. Batchelor, Phys. Fluids **12**, 233 (1969).
[3] U. Frisch and P.-L. Sulem, Phys. Fluids **27**, 1921 (1984).
[4] J. R. Herring and J. C. McWilliams, J. Fluid Mech. **153**, 229 (1985).
[5] M. E. Maltrud and G. K. Vallis, J. Fluid Mech. **228**, 321 (1991).
[6] S. Sukorianski, B. Galperin, and A. Chekhlov, Phys. Fluids **11**, 3043 (1999).
[7] S. Chen, R. E. Ecke, G. L. Eyink, M. Rivera, M. Wan, and Z. Xiao, Phys. Rev. Lett. **96**, 084502 (2006).
[8] J. Paret and P. Tabeling, Phys. Rev. Lett. **79**, 4162 (1997).
[9] A. Babiano, B. Dubrulle, and P. Frick, Phys. Rev. E **52**, 3719 (1995).
[10] E. Lindborg and K. Alvelius, Phys. Fluids **12**, 945 (2000).
[11] C. Pasquero and G. Falkovich, Phys. Rev. E **65**, 056305 (2002).
[12] S. Chen, R. E. Ecke, G. L. Eyink, X. Wang, and Z. Xiao, Phys. Rev. Lett. **91**, 214501 (2003).

[13] J. Paret, M. C. Jullien, and P. Tabeling, Phys. Rev. Lett. **83**, 3418 (1999).
[14] C. V. Tran and J. C. Bowman, Phys. Rev. E **69**, 036303 (2004).
[15] C. V. Tran and T. G. Shepherd, Physica D **165**, 199 (2002).
[16] V. Borue, Phys. Rev. Lett. **72**, 1475 (1994).
[17] L. M. Smith and V. Yakhot, J. Fluid Mech. **274**, 115 (1994).
[18] G. F. Carnevale, J. C. McWilliams, Y. Pomeau, J. B. Weiss, and W. R. Young, Phys. Rev. Lett. **66**, 2735 (1991).
[19] R. Benzi, M. Collela, M. Briscolini, and P. Santangelo, Phys. Fluids A **4**, 1036 (1992).
[20] J. B. Weiss and J. C. McWilliams, Phys. Fluids A **5**, 608 (1993).
[21] S. Danilov and D. Gurarie, Phys. Rev. E **63**, 020203(R) (2001); **63**, 061208 (2001).
[22] C. V. Tran, Physica D **191**, 137 (2004).
[23] M. A. Rutgers, Phys. Rev. Lett. **81**, 2244 (1998).
[24] M. E. Maltrud and G. K. Vallis, Phys. Fluids A **5**, 1760 (1993).